Volume 27
Number 36
28 September 2025
Pages 5929–6080

CrystEngComm

rsc.li/crystengcomm

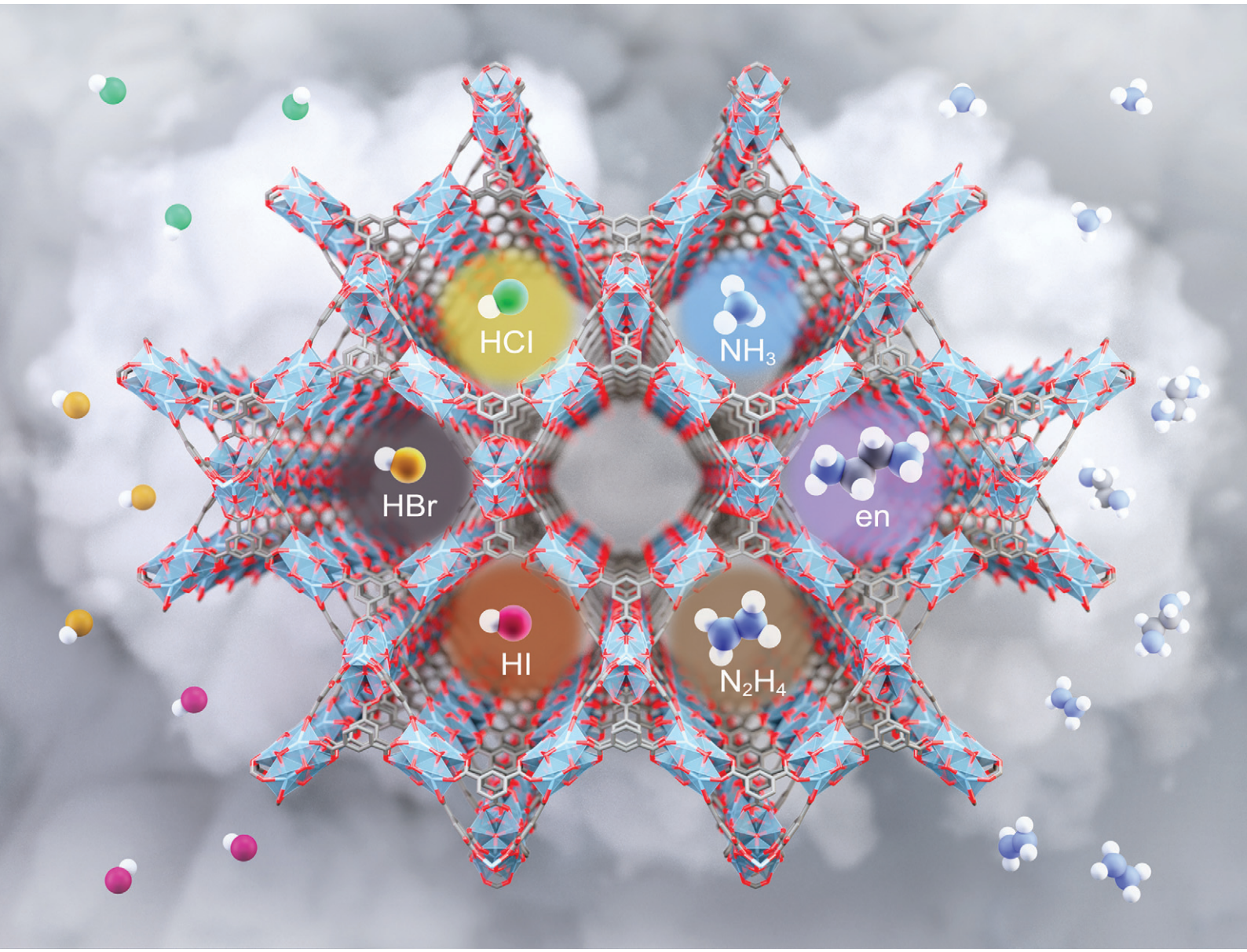

ISSN 1466-8033

ROYAL SOCIETY OF CHEMISTRY

PAPER

Jin Yeong Kim *et al.*

Ligand-responsive MOF-based colourimetric sensor for visual identification of colourless corrosive acid and base vapours

CrystEngComm

ROYAL SOCIETY OF CHEMISTRY

PAPER

View Article Online
View Journal | View Issue

Cite this: *CrystEngComm*, 2025, **27**, 5965

Ligand-responsive MOF-based colourimetric sensor for visual identification of colourless corrosive acid and base vapours

Hyejin Yoo, Chanhyun Park, Solmin Lee and Jin Yeong Kim *

Received 24th June 2025,
Accepted 30th July 2025

DOI: 10.1039/d5ce00640f

rsc.li/crystengcomm

The development of reliable sensors for identifying corrosive vapours remains a significant challenge due to the high reactivity of these gases and the fundamentally distinct sensing mechanisms required for acids and bases. Herein, we report a single-component colourimetric sensor based on Cu^{2+}-functionalised MOF-808 (Cu-MOF-808) capable of visually distinguishing six representative corrosive vapours, including hydrogen halides (HCl, HBr, HI) and volatile amines (NH_3, ethylenediamine, N_2H_4). Cu^{2+} ions were post-synthetically anchored onto the Zr_6 nodes of the robust MOF-808 framework, providing accessible and reactive sites for vapour-responsive colour changes. The sensor exhibited distinct, analyte-specific colour transitions upon vapour exposure while remaining stable under variations in humidity, temperature, and common interfering gases. For practical application, Cu-MOF-808 was embedded in a flexible PVDF matrix to fabricate a portable sensor film. Upon vapour exposure, colour changes were digitised into RGB values and accurately classified within 15 seconds *via* statistical analysis. These results highlight the potential of Cu-MOF-808 as a practical sensor for real-time monitoring of corrosive gases in the real-world.

1. Introduction

Corrosive chemicals, such as hydrogen halides (HCl, HBr, HI) and volatile bases (NH_3, ethylenediamine, N_2H_4) are used in diverse industrial applications, including polymer synthesis, metal processing, fertilizer production, pharmaceuticals, semiconductor fabrication, and chemical synthesis.[1–6] These substances are highly reactive and can cause severe damage to both metallic and organic materials upon contact.[7–9] Owing to their toxicity and corrosive nature, accidental leaks pose serious risks to human health and infrastructure.[4,10–14] Emergency response and mitigation strategies depend on the specific identity of the released gas, making accurate and rapid identification a matter of critical importance.[14–16] However, the strong reactivity of these gases often leads to degradation or failure of electronic circuit-based gas sensors, limiting their reliability in real-world applications.[17,18]

Colourimetric sensing offers an elegant, circuit-free alternative that converts chemical interactions into visible signals recognizable by the naked eye or a simple camera. Recent studies have introduced various colourimetric sensors for detecting corrosive vapours, employing materials such as organic dyes,[5,6,19–24] polymers,[2,25–27] molecular metal complexes,[28–31] covalent organic frameworks (COFs),[32–34] and metal–organic frameworks (MOFs).[4,35–40] However, most reported systems are limited to either acidic or basic gases, as their distinct donor-acceptor properties often require separate recognition mechanisms and functional groups. Recent research on colourimetric sensor arrays has shown that combining responses from multiple sensing elements can differentiate various chemical vapours, including certain corrosive acid and base gases, though this approach demands more complex data analysis.[41,42] As a result, although corrosive gases are important targets, the development of sensor materials that can visually detect them is still in its early stages.

A promising strategy for decoding multiple colourless corrosive vapours is to employ transition metal ions, which are well known to form distinctly coloured complexes with acidic and basic analytes in solution. However, the intrinsically nonporous nature of most such complexes limits gas-phase accessibility, reducing their effectiveness in practical sensing applications. Interestingly, recent studies have attempted to overcome the nonporous limitations of metal ions by immobilizing single metal ions within porous matrices including porous carbons,[43,44] COFs,[45,46] and MOFs,[47–51] thereby exposing them directly to the external environment for applications in catalysis or single-gas sensing. However, these approaches have not yet been extended to the development of decoding sensors for a broad range of corrosive gases.

In this study, we report a single-component colourimetric sensor that enables identification of both corrosive acid and

Department of Chemistry Education, Seoul National University, Seoul 08826, Republic of Korea. E-mail: jykim@snu.ac.kr

base vapours using a Cu^{2+}-functionalized metal–organic framework, Cu-MOF-808. The Cu^{2+} ions are anchored directly onto the Zr_6 clusters of the robust MOF-808, $(Zr_6O_4(OH)_4(BTC)_2(HCOO)_6$, where BTC = 1,3,5-benzenetricarboxylic acid), forming readily accessible colourimetric sites that interact with target gases. Given the colour sensitivity of Cu^{2+} to changes in oxidation state and ligand field, each of the six tested gases—HCl, HBr, HI, NH_3, ethylenediamine, and N_2H_4—induces a distinct colour change, while remaining unresponsive to common interfering gases, humidity variations, and thermal fluctuations. By incorporating a flexible polymer, Cu-MOF-808 was effectively fabricated into a compact, portable device for detecting corrosive gases. This device displays noticeable colour changes visible to the naked eye and can be tracked by camera sensors, demonstrating its practical utility and adaptability for continuous, 24-hour on-site colourimetric monitoring of corrosive vapours.

2. Results and discussion

2.1. Preparation and characterisation of Cu-MOF-808

To prepare a colourimetric sensor for corrosive vapour detection, the robust and porous Zr-based MOF-808 was functionalized with Cu^{2+} ions as colourimetric centre, *via* previously reported procedures.[49,52] Cyan-coloured Cu^{2+}-incorporated MOF-808 powder was obtained by immersing acid-activated MOF-808, bearing labile H_2O and –OH groups on its Zr_6 nodes that facilitate coordination with various transition-metal cations,[49–51,53,54] into $Cu(CH_3COO)_2$ solution (68 mg, 0.34 mmol in 10 mL of methanol) for overnight at 60 °C. Notably, the cyan colour persisted even after repeated washing with distilled water, without returning to the original white colour of MOF-808 (Fig. 1a), supports that the Cu^{2+} ions are strongly coordinated to the Zr_6 clusters within MOF framework rather than being merely physically adsorbed. The structural integrity of MOF-808 after copper incorporation was confirmed by X-ray powder diffraction (XRPD) (Fig. 1b and S1), while scanning electron microscopy (SEM) images showed no significant morphological changes (Fig. S2). The molar ratio of Cu to Zr was determined to be 0.62 using inductively coupled plasma-atomic emission spectroscopy (ICP-AES), corresponding to the incorporation of approximately 3.69 Cu ions per Zr_6 cluster (Table S1). In addition, energy dispersive X-ray spectroscopy (EDS) mapping confirmed the homogeneous distribution of copper throughout the MOF structure (Fig. 1d). Furthermore, nitrogen sorption analysis revealed reduced surface area and pore size of 1000 $m^2\ g^{-1}$ and 1.30 nm, respectively, compared to the pristine MOF-808 (1697 $m^2\ g^{-1}$ and 1.59 nm), indicating partial pore occupation by anchoring Cu^{2+} ions but retained porosity sufficient for vapour access (Fig. 1c and S3). These results collectively confirm the successful synthesis of Cu-MOF-808 with structurally integrated Cu^{2+} sites while maintaining accessible pores, thereby enabling its application as a colourimetric sensor for corrosive vapours.

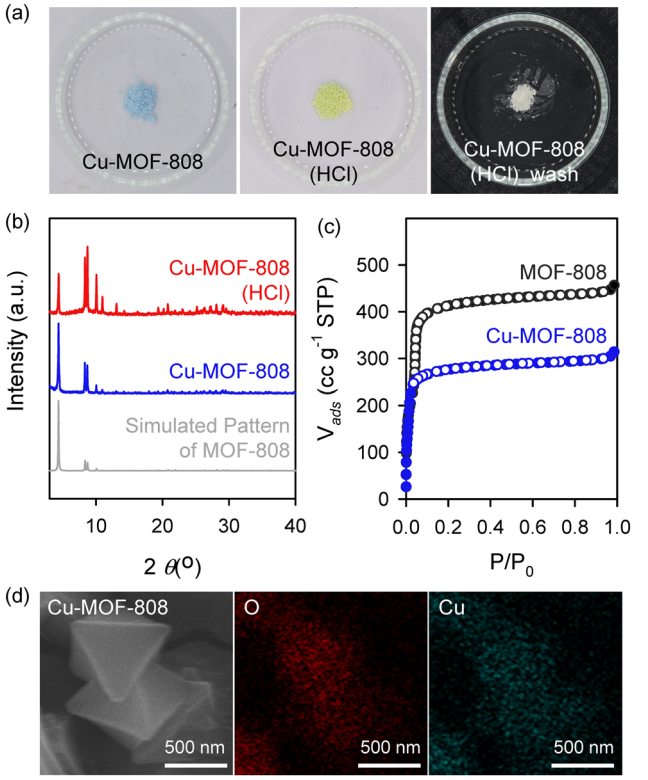

Fig. 1 (a) Photographs of Cu-MOF-808 (left) and hydrochloric acid (HCl) exposed Cu-MOF-808 (centre), and Cu-MOF-808 exposed to HCl and subsequently washed with water (right). (b) XRPD patterns of Cu-MOF-808 (blue) and Cu-MOF-808 (HCl) (red) with simulated XRPD pattern of MOF-808 (grey). (c) N_2 sorption isotherms of MOF-808 (black) and Cu-MOF-808 (blue) measured at 77 K. (d) SEM image (left) and EDS elemental mapping (centre and right) of Cu-MOF-808.

2.2. Colourimetric response of Cu-MOF-808 to HCl vapour

Preliminary evaluation of the responsiveness of Cu-MOF-808 was carried out by exposing the samples to corrosive HCl vapor generated from a concentrated hydrochloric acid solution. Upon exposure to HCl vapour, Cu-MOF-808 underwent a rapid and visually distinct colour change from cyan to yellow within 20 seconds, enabling immediate naked-eye recognition (Fig. 1a). Importantly, no structural and morphological changes were observed in the MOF-808 framework (Fig. 1b and S2), confirming that the colour transition did not result from framework degradation. Washing the HCl-exposed Cu-MOF-808 with water resulted in a white powder, rather than restoring the cyan colour, suggesting Cu^{2+} dissociation from the Zr_6 clusters and possible limitations in reusability (Fig. 1a and S4). The ultraviolet-visible near-infrared (UV-vis-NIR) spectrum of HCl-exposed Cu-MOF-808 revealed new absorption bands at 33 898 and 25 907 cm^{-1}, corresponding to ligand-to-metal charge transfer (LMCT) transitions in tetrahedral $[CuCl_4]^{2-}$ species,[1,55–57] confirming that released free Cu^{2+} ions formed yellow Cu–Cl complexes (Fig. S4b). To further probe the dissociation mechanism, Cu-MOF-808 was immersed in three 4 M Cl^- aqueous solutions: neutral NaCl and KCl, and acidic HCl. A light-yellow colour developed only in the HCl solution,

whereas the material retained its original cyan colour in the neutral solutions (Fig. S5). This observation suggests that two factors are both essential for the colorimetric response to occur: the protonation of the $Zr_6O_4(OH)_4$ clusters under acidic conditions, which facilitates the release of free Cu^{2+} ions,[58] and the presence of Cl^- ions to subsequently form yellow $[CuCl_4]^{2-}$ complexes.[40]

Furthermore, Cu-MOF-808 exhibited the ability to detect HCl vapor at concentrations as low as 120 ppm, albeit with a longer response time. In contrast, the non-porous reference compound $Cu(CH_3COO)_2$ showed no discernible colour change even after 1 hour of exposure, whereas the faster response observed for Cu-MOF-808 highlights the importance of accessible Cu^{2+} sites within the porous framework for efficient colorimetric sensing (Fig. S6). Notably, Cu-MOF-808 displayed high selectivity toward HCl vapour, as evidenced by its retention of original cyan colour after 24 hours of exposure to potential interferents, including N_2, O_2, CO_2, and environmental variations in humidity and temperature (Fig. 2 and S7). These results demonstrate negligible response to non-target species, highlighting its practical potential as a reliable and selective platform for detecting corrosive vapours under ambient conditions.

2.3. Colourimetric response to various corrosive vapours

Building upon the established mechanism for HCl-induced colour change, in which protonation facilitates the dissociation of Cu^{2+} ions from Zr_6 clusters and enables subsequent coordination with halide anions to produce distinct colours, we extended our investigation to other corrosive acid vapours. Upon exposure to HBr and HI vapours, Cu-MOF-808 showed distinct colour changes from cyan to deep purple and yellowish-brown, respectively (Fig. 2). Specifically, UV-vis-NIR spectra of Cu-MOF-808 after exposure to HBr revealed absorption bands at 28 249 cm^{-1} and 19 121 cm^{-1}, corresponding to absorption bands of purple $[CuBr_4]^{2-}$ complex, supporting the formation of Cu–Br coordination species (Fig. S8).[56] In contrast, HI exposure induced a more complex response involving both coordination and redox chemistry. X-ray powder diffraction (XRPD) confirmed the formation of white CuI(s), while UV-vis-NIR spectra indicated an absorption band at 34 247 and 27 174 cm^{-1}, indicating the presence of brown I_3^- (Fig. S9).[59] These results suggest that the yellowish-brown colour observed upon HI exposure originates primarily from I_3^-, rather than the Cu–I coordination complex. Interestingly, these colour changes are consistent with the reported colorimetric responses of free Cu^{2+} ions upon interaction with corrosive acid vapours,[40] supporting that the colorimetric response of Cu-MOF-808 is governed by proton-triggered Cu^{2+} release followed by anion-dependent coordination. This mechanism enables Cu-MOF-808 to produce distinct colorimetric signatures for different acid vapours, thereby allowing their identification.

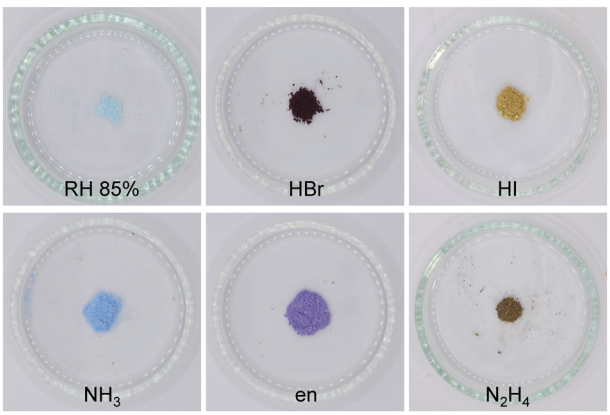

Fig. 2 Photographs of Cu-MOF-808 after 24-hour-exposure to 85% relative humidity (RH) for 24 hours, and five corrosive vapours: HBr, HI, NH_3, ethylenediamine (en), and N_2H_4.

Motivated by previous reports indicating that some coordination sites on the Cu^{2+} centres of the Zr_6 clusters are occupied by labile H_2O molecules,[48] which can be readily displaced by stronger ligands, we extended our investigation to non-acidic corrosive vapours. Corrosive amines are known to exhibit higher binding affinities and stronger ligand fields than H_2O,[60–62] making them suitable candidates to replace the coordinated water and form distinct Cu–amine complexes with characteristic colours. To test this hypothesis, Cu-MOF-808 was exposed to three representative amines: ammonia (NH_3), ethylenediamine (en), and hydrazine (N_2H_4). As expected, NH_3 exposure induced a visible colour shift from cyan to blue (Fig. 2). This was accompanied by the emergence of a new N–H stretching band at 1612 cm^{-1} in the IR spectrum and a blue-shifted absorption band near 15 000 cm^{-1} in the UV-vis-NIR spectrum—both consistent with Cu–NH_3 complex formation (Fig. S9).[54,63–66] Exposure to ethylenediamine, a stronger bidentate ligand, resulted in a purple colour change and a blue-shifted absorption band at ~17 000 cm^{-1} in the UV-vis-NIR spectrum, suggestive of Cu–en chelation (Fig. 2 and S11). Conversely, exposure to N_2H_4, a potent reducing agent, resulted in a significant colour change from cyan to dark brown (Fig. 2). This change is attributed to the reduction of Cu^{2+}, as confirmed by the approximately 2 eV red-shifted binding energy of Cu $2p_{3/2}$ in X-ray photoelectron spectroscopy (XPS) (Fig. S12). Collectively, these results underscore the unique capability of a single MOF platform to selectively distinguish both corrosive acids and amines *via* distinct ligand-induced colorimetric signatures, highlighting its potential as a versatile, all-in-one sensor for diverse corrosive vapours.

2.4. Portable Cu-MOF-808 sensor and multivariate vapour discrimination

To translate the observed colourimetric responses into a practical sensing platform, a portable sensor was fabricated by integrating Cu-MOF-808 into a poly(vinylidene fluoride) (PVDF) matrix. As previously reported, this strategy enables

high MOF loading while preserving the accessibility of active sites to the surrounding environment.[67,68] The sensor was prepared by drop-casting a Cu-MOF-808-based ink containing 5 wt% PVDF onto a 5 mm diameter glass substrate, yielding a flexible and easily handled device. Upon exposure to HCl vapour, the sensor exhibited a distinct colour change from cyan to yellow, consistent with that observed in the powder form. This transition was clearly detectable by both the naked eye and a camera sensor and was quantitatively analysed through RGB channel values (Fig. 3a), enabling 24-hour real-time monitoring of colourimetric response. Notably, at low concentration, the sensor exhibited an attenuated colour change from cyan to yellow over the same exposure period, indicating its potential for quantitative detection (Fig. S13). This colour change was quantified as $|\Delta B|/B_0$, where $|\Delta B|$ is the absolute change in the blue channel value and B_0 is the initial blue channel value. A linear calibration curve was obtained in the range of 160–745 ppm, with a calculated limit of detection (LOD) of 89 ppm (S/N = 3), confirming the applicability of the sensor for HCl quantification. Furthermore, to assess environmental stability, the sensor was subjected to humid conditions (85% relative humidity for 24 h). No discernible colour change was observed, either visually or in the RGB data (Fig. 3b), indicating strong resistance to humidity and further supporting the sensor's practicality for selective corrosive gas detection.

Building on these findings, we further evaluated the sensor's response to six additional corrosive vapours. Each analyte produced a unique RGB profile (Fig. 3c and S14), enabling visual differentiation. To statistically validate this selectivity, principal component analysis (PCA) and hierarchical cluster analysis (HCA) was applied to the RGB difference values (dR, dG, dB) obtained after 15 seconds of exposure. Despite the short exposure time, insufficient for naked-eye recognition, the algorithm successfully classified all vapours without overlap or misclassification (Fig. S15). To assess identification capability for unknowns, RGB datasets from unknown samples A and B were included in the HCA library (Fig. 3d). The results revealed that samples A and B corresponded to HBr and en, respectively. Together, these results highlight the practical potential of the fabricated portable Cu-MOF-808 sensor as a reliable and accessible platform for the visual detection and identification of corrosive vapours under ambient conditions.

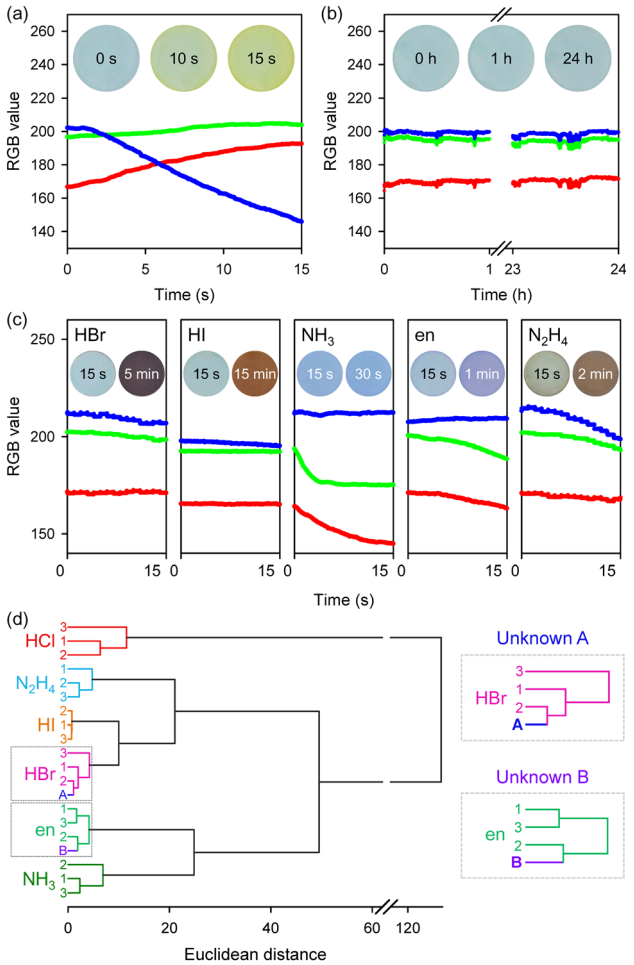

Fig. 3 (a) Time-dependent RGB curves of Cu-MOF-808 portable sensors with 5 wt% PVDF under HCl vapour. Inset: photographs of Cu-MOF-808 portable sensor after exposure to HCl vapour for 0 s (left), 10 s (centre), and 15 s (right), respectively. (b) Time-dependent RGB curves of Cu-MOF-808 portable sensor under 85% RH for 24 hours. Inset: photographs of Cu-MOF-808 portable sensor under 85% RH conditions. (c) Time-dependent RGB curves of Cu-MOF-808 portable sensor under HBr, HI, NH_3, en, and N_2H_4 vapours. Inset: photographs of Cu-MOF-808 portable sensor exposure to HBr, HI, NH_3, en, and N_2H_4 vapours for 15 s (left), and 5 min, 15 min, 30 s, 1 min, 2 min, respectively (right). (d) Hierarchical cluster analysis (HCA) dendrogram generated from RGB datasets (dR, dG, dB) of Cu-MOF-808 upon exposure to six different corrosive vapours, based on three trials and two unknown sample. Inset: classification results of two unknown samples (A and B) using the established HCA library.

Conclusions

In conclusion, we present a Cu-MOF-808-based colourimetric sensor platform for corrosive vapour identification, in which post-synthetically anchored Cu^{2+} ions on Zr_6 clusters act as reactive, colour-responsive centres. This single-component system enabled the visual identification of six corrosive vapours, including hydrohalic acids and volatile bases, *via* distinct ligand-induced colour changes. The unified sensing mechanism, driven by coordination or redox interactions at the Cu^{2+} sites, allows for discrimination of both acidic and basic vapours within a single framework, overcoming the limitations of traditional acid/base-specific sensors. Furthermore, integration into a flexible PVDF matrix enabled the fabrication of a miniaturized portable sensor. Upon vapour exposure, the colour changes of the sensor were quantified into RGB datasets *via* digital analysis and HCA enabled rapid and accurate classification of all tested vapours, including unknowns, within 15 seconds. These findings underscore the practical applicability of Cu-MOF-808 as a selective, portable, and rapid-response sensor for real-time on-site corrosive vapour monitoring.

Author contributions

H. Y. and J. Y. K. conceptualized the study and designed the experiments. H. Y. synthesised the molecular structure, carried out the experimental work and analysed the data; C. P. helped the experimental work. S. L. helped in the N_2 sorption isotherms. H. Y. and J. Y. K. co-wrote the manuscript. All authors discussed and analysed the results.

Conflicts of interest

There are no conflicts to declare.

Data availability

Supplementary Information is available: The SI contains additional experimental details, characterization data (*e.g.*, XRPD, SEM, pore size distribution, UV-vis-NIR, FT-IR, and XPS), and supporting figures referenced in the main text. See DOI: **https://doi.org/10.1039/D5CE00640F**.

The data supporting this article have been included as part of the SI.

Acknowledgements

This work was supported by a National Research Foundation of Korea grant (NRF-2022R1C1C101022013), a Korea Basic Science Institute grant (RS-2024-00405170), and the BK21 FOUR Program through the Centre for Science Education in the Infosphere.

Notes and references

1 X. Chen, H. Hu, Z. Xia, W. Gao, W. Gou, Y. Qu and Y. Ma, *J. Mater. Chem. C*, 2017, **5**, 309–313.
2 S. Kingchok, J. Siriboon, L. Sun, T. A. P. Seery, N. Traiphol and R. Traiphol, *ACS Appl. Nano Mater.*, 2022, **5**, 4146–4156.
3 H. L. Noh, Y. K. Park, B. M. Oh, J. Zheng, S.-H. Kim, W. Lee and J. H. Kim, *Sens. Actuators, B*, 2019, **301**, 127079.
4 T. Leelasree, M. Dixit and H. Aggarwai, *Chem. Mater.*, 2023, **35**, 416–423.
5 H. Wang, W. Yin, H. Ma, X. He, G. Yin and W. Huang, *Spectrochim. Acta, Part A*, 2023, **302**, 123004.
6 X. Yang, J. Zhou, Y. Li, M. Yan, Y. Cui and G. Sun, *Spectrochim. Acta, Part A*, 2020, **240**, 118539.
7 M. H. Brown, W. B. DeLong and J. R. Auld, *Ind. Eng. Chem.*, 1947, **39**, 839–844.
8 C.-W. Zhao, J.-P. Ma, Q.-K. Liu, X.-R. Wang, Y. Liu, J. Yang, J.-S. Yang and Y.-B. Dong, *Chem. Commun.*, 2016, **52**, 5238–5241.
9 Z.-H. Zhu, Z. Ni, H.-H. Zh, G. Feng and B. Z. Tang, *Adv. Funct. Mater.*, 2021, **31**, 2106925.
10 D. Kwak, Y. Lei and R. Maric, *Talanta*, 2019, **204**, 713–730.
11 C. M. R. Almeida, J. M. C. S. Magalhães, M. F. Barroso and L. Durães, *J. Mater. Chem. C*, 2022, **10**, 15263–15276.
12 Y. Hua and X. Ou, *J. Burn Care Res.*, 2024, **45**, 250–252.
13 B. Masia, M. Yang and V. Cozzani, *ACS Chem. Health Saf.*, 2024, **31**, 503–520.
14 R. P. Pangeni, B. Timilsina, P. R. Oli, S. Khadka and P. R. Regmi, *Ann. Med. Surg.*, 2022, **82**, 104741.
15 W. E. Luttrell, *ACS Chem. Health Saf.*, 2002, **9**, 30–31.
16 S. L. Rose-Pehrsson, R. E. Shaffer, S. J. Hart, F. W. Williams, D. T. Gottuk, B. D. Strehlen and S. A. Hill, *Sens. Actuators, B*, 2000, **69**, 325–335.
17 S. Panda, S. Mehlawat, N. Dhariwal, A. Kuma and A. Sanger, *Mater. Sci. Eng., B*, 2024, **308**, 117616.
18 A. U. Malik, F. Al-Muaili, M. Al-Ayashi and A. Meroufel, *Case Stud. Eng. Fail. Anal.*, 2013, **1**, 200–208.
19 Y. J. Diaz, Z. A. Page, A. S. Knight, N. J. Treat, J. R. Hemmer, C. J. Hawker and J. R. de Alaniz, *Chem. – Eur. J.*, 2017, **23**, 3562–3566.
20 G. Zhang, A. S. Loch, J. C. M. Kistemaker, P. L. Burn and P. E. Shaw, *J. Mater. Chem. C*, 2020, **8**, 13723–13732.
21 Y.-S. Nam, I. Yoo, O. Yarimaga, I. S. Park, D.-H. Park, S. Song, J.-M. Kim and C. W. Lee, *Chem. Commun.*, 2014, **50**, 4251–4254.
22 J. Guo, X. Wei, X. Fang, R. Shan and X. Zhang, *Sens. Actuators, B*, 2021, **347**, 130623.
23 M. E. Genovese, G. Caputo, G. Nanni, C. Setti, M. Bustreo, G. Perotto, A. Athanassiou and D. Fragouli, *ACS Appl. Mater. Interfaces*, 2017, **9**, 40707–40715.
24 K. Li, J. Cui, Z. Yang, Y. Huo, W. Duan, S. Gong and Z. Liu, *Dalton Trans.*, 2018, **47**, 15002–15008.
25 D. Wilkinson, D. Taylor, N. B. McKeown and G. Cooke, *RSC Appl. Polym.*, 2025, **3**, 701–710.
26 K. P. Subodh and D. T. Masram, *J. Mater. Chem. C*, 2020, **8**, 9201–9204.
27 K. P. Subodh and D. T. Masram, *Dalton Trans.*, 2020, **49**, 1007–1010.
28 G. M. Espallargas, L. Brammer, J. van de Streek, K. Shankland, A. J. Florence and H. Adams, *J. Am. Chem. Soc.*, 2006, **128**, 9584–9585.
29 Q.-F. Liang, H.-W. Zheng, D.-D. Yang and X.-J. Zheng, *Cryst. Growth Des.*, 2022, **22**, 3924–3931.
30 D.-D. Yang, X.-H. Ning, H.-W. Zheng, Y.-S. Shi, B. Jin, T. Xiao and X.-J. Zheng, *Dyes Pigm.*, 2023, **212**, 111149.
31 Q.-F. Liang, H.-W. Zheng, D.-D. Yang and X.-J. Zheng, *CrystEngComm*, 2022, **24**, 543–551.
32 P. K. Kundu, G. L. Olsen, V. Kiss and R. Klajn, *Nat. Commun.*, 2014, **5**, 3588.
33 A. Laura, E. W. Evans, J. Gorman, S. Orsborne, D. Bessinger, T. Bein, R. H. Friend and F. Auras, *J. Am. Chem. Soc.*, 2019, **141**(39), 15693–15699.
34 W. Gong, C. Liu, H. Shi, M. Yin, W. Li, Q. Song, Y. Dong and C. Zhang, *J. Mater. Chem. C*, 2022, **10**, 3553–3559.
35 S. Qin, M. Chen and L. Wu, *J. Mater. Chem. A*, 2022, **10**, 21072–21079.
36 J. Othong, J. Boonmak, N. Wannarit, F. Kielar, T. Puangmali, W. Phanchai and S. Youngme, *Sens. Actuators, B*, 2021, **343**, 130066.
37 A. Mallick, B. Garai, M. A. Addicoat, P. St, T. H. Petkov and R. Banerjee, *Chem. Sci.*, 2015, **6**, 1420–1425.

38 Z. H. Zhu, Z. Ni, H. H. Zou, G. Feng and B. Z. Tang, *Adv. Funct. Mater.*, 2021, **31**, 2106925.
39 R. Goswami, S. Das, N. Seal, B. Pathak and S. Neogi, *ACS Appl. Mater. Interfaces*, 2021, **13**, 34012–34026.
40 W. Jang, H. Yoo, D. Shin, S. Noh and J. Y. Kim, *Nat. Commun.*, 2025, **16**, 385.
41 L. Feng, C. J. Musto, J. W. Kemling, S. H. Lim, W. Zhong and K. S. Suslick, *Anal. Chem.*, 2010, **82**, 9433–9440.
42 K. Jin, D. Moon, Y.-P. Chen and J. Park, *Adv. Mater.*, 2024, **36**, 2309570.
43 M. Shen, J. Qi, K. Gao, C. Duan, J. Liu, Q. Liu, H. Yang and Y. Ni, *Chem. Eng. J.*, 2023, **464**, 142719.
44 X. Zhu, Y. Xu, L. Ran, S. Chen and X. Qiu, *Inorg. Chem.*, 2024, **63**, 3893–3900.
45 L. Ran, Z. Li, B. Ran, J. Cao, Y. Zhao, T. Shao, M. K. H. Leung, L. Sun and J. Hou, *J. Am. Chem. Soc.*, 2022, **144**, 17097–17109.
46 V. Hasija, S. Patial, P. Raizada, A. A. P. Khan, A. M. Asiri, Q. V. Le, V.-H. Nguyen and P. Singh, *Coord. Chem. Rev.*, 2022, **452**, 214298.
47 A. M. Abdel-Mageed, B. Rungtaweevoranit, M. Parlinska-Wojtan, X. Pei, O. M. Yaghi and R. J. Behm, *J. Am. Chem. Soc.*, 2019, **141**, 5201–5210.
48 N. Marquardt, M. Dahlke and D. A. Schaate, *ChemPlusChem*, 2023, **88**, e202300109.
49 I. del Castillo-Velilla, A. Sousaraei, I. Romero-Muñiz, C. Castillo-Blas, A. S. J. Méndez, F. E. Oropeza, V. A. de la Peña O'Shea, J. Cabanillas-González, A. Mavrandonakis and A. E. Platero-Prats, *Nat. Commun.*, 2023, **14**, 2506.
50 X. He, B. G. Looker, K. T. Dinh, A. W. Stubbs, T. Chen, R. J. Meyer, P. Serna, Y. Román-Leshkov, K. M. Lancastser and M. Dincă, *ACS Catal.*, 2020, **10**, 7820–7825.
51 Y. Zhu, J. Zheng, J. Ye, Y. Cui, K. Koh, L. Kovarik, D. M. Camaioni, J. L. Fulton, D. G. Truhlar, M. Neurock, C. J. Cramer, O. Y. Gutiérrez and J. A. Lercher, *Nat. Commun.*, 2020, **11**, 5849.
52 J. Jiang, F. Gándara, Y.-B. Zhang, K. Na, O. M. Yaghi and W. G. Klemperer, *J. Am. Chem. Soc.*, 2014, **136**, 12844–12847.
53 C. Castillo-Blas, I. Romero-Muñiz, A. Mavrandonakis, L. Simonelli and A. E. Platero-Prats, *Chem. Commun.*, 2020, **56**, 15615–15618.
54 Y. Ma, W. Lu, X. Han, Y. Chen, I. da Silva, D. Lee, A. M. Sheveleva, Z. Wang, J. Li, W. Li, M. Fan, S. Xu, F. Tuna, E. J. L. Mclnnes, Y. Cheng, S. Rudić, P. Manuel, M. D. Frogley, A. J. Ramirez-Cuesta, M. Schröder and S. Yang, *J. Am. Chem. Soc.*, 2022, **144**, 8624–8632.
55 L. Helmholz and R. F. Kruh, *J. Am. Chem. Soc.*, 1952, **74**, 1176–1181.
56 C. Furlani and G. Morpurgo, *Theor. Chim. Acta*, 1963, **1**, 102–115.
57 A. S. Mereshchlenko, P. K. Olshin, A. M. Karimov, M. Y. Skripkin, K. A. Burkov, Y. S. Tveryanovich and A. N. Tarnovsky, *Chem. Phys. Lett.*, 2014, **615**, 105–110.
58 I. del Castillo-Velilla, I. Romero-Muñiz, C. Marini, C. Montoro and A. E. Platero-Prats, *Nanoscale*, 2024, **16**, 6627–6635.
59 A. Apostolopoulou, A. Margalias and E. Stathatos, *RSC Adv.*, 2015, **5**, 58307–58315.
60 N. Nijern, K. Fürsich, H. Bluhm, S. R. Leone and M. K. Gilles, *J. Phys. Chem. C*, 2015, **119**, 24781–24788.
61 A. Bérces, T. Nukada, P. Margi and T. Ziegler, *J. Phys. Chem. A*, 1999, **103**, 9693–9701.
62 A. T. Baker, *J. Chem. Educ.*, 1998, **75**, 98.
63 L. Wang, W. Li, G. Qi and D. Weng, *J. Catal.*, 2012, **289**, 21–29.
64 D. Wang, L. Zhang, K. Kamasamudran and W. S. Epling, *ACS Catal.*, 2013, **3**, 871–881.
65 S. Bashkova and T. J. Bandosz, *J. Colloid Interface Sci.*, 2014, **417**, 109–114.
66 K. I. Hadjiivanov, D. A. Panayotov, M. Y. Mihaylov, E. Z. Ivanova, K. K. Chakarova, S. M. Andonova and N. L. Drenchev, *Chem. Rev.*, 2021, **121**, 1286–1424.
67 M. S. Denny Jr. and S. M. Cohen, *Angew. Chem., Int. Ed.*, 2015, **54**, 9029–9032.
68 J. B. DeCoste, M. S. Denny Jr., G. W. Peterson, J. J. Mahle and S. M. Cohen, *Chem. Sci.*, 2016, **7**, 2711–2716.

